JMEPEG (1998) 7:727-732

The Effects of a CeO_2 Coating on the Corrosion Parameters of Type 304 Stainless Steel

R.G. Biswas and R.D. Sanders

(Submitted 10 July 1997; in revised form 29 April 1998)

Coatings of CeO_2 derived from inorganic sol-gel dispersions were applied to type 304 bright annealed stainless steel (British Standard 1449 type 304S31) coupons and subjected to heat treatments at 450 and 550 °C. The coatings, 0.5 μm thick, were transparent, adherent, and stable. The aqueous corrosion properties of the coated coupons in 1 molar NaCl were then studied by potentiodynamic polarization measurements and electrochemical impedance spectroscopy. The derived corrosion parameters were then compared with similarly heat-treated, uncoated 304SS coupons. The results indicate that the application of a CeO_2 coating, heat treated at 550 °C, improves the corrosion rate as compared to an uncoated heat-treated coupon. The polarization curve for the 450 °C heat-treated, coated coupon showed passive behavior compared to transpassive for the uncoated specimen. The impedance spectrum data for the uncoated, as-received coupon could be modeled using a resistor in series with a parallel capacitor resistor combination "Randles" equivalent circuit. A coated coupon, heat treated at 550 °C, could be modeled using a more complex equivalent circuit involving a constant phase element, due to the CeO_2 coating. Modeling of the impedance characteristics for the oxidized coupons required the addition of a second series element consisting of a parallel resistor capacitor combination to give a Chi square statistic fit of $\chi^2 < 5 \times 10^{-4}$.

Keywords coatings, corrosion, impedance

1. Introduction

The use of ceramic coatings to provide protection from harsh environments is of major industrial significance (Ref 1, 2). The application of the ceramic coating is directly related to the nature of the ceramic, such as high thermal stability, high hardness, chemical inertness, and density. This gives rise to three principle types of coatings: (a) thermal barrier coatings; (b) wear-resistant coatings; and (c) corrosion-resistant coatings. Ceramic coatings may be applied by chemical vapor deposition, physical vapor deposition, thermal spraying, and sol-gel techniques. Sol-gel technology is widely used for preparation of oxide materials (Ref 3) from solutions containing inorganic or metal organic precursors that are hydrolyzed to form inorganic polymers and colloids. Sol-gel also has the advantages of low-temperature processing, cheap coating technology, material economies, the application of multi-component oxides, and the ability to coat complex shapes and a variety of substrate materials, compared to other deposition techniques. Coatings can be applied by spin coating or dip coating, or by electrophoresis with the process repeated to build up coatings with thicknesses of up to tens of microns. Disadvantages of the sol-gel deposition of coatings are that the sol morphology must be carefully controlled to ensure continuous films, and that the films require drying and densifying heat treatments which may be detrimental to the substrate.

Electrochemical corrosion measurements allow quick determination of coating and metal performance. Although capable of obtaining corrosion parameters such as corrosion rate (CR) and open circuit potential (OCP), direct-current electrochemical measurement techniques are unable to give information about the rate of the different corroding mechanisms and coating performance (e.g., porosity). These parameters may be found using alternating signal techniques, such as electrochemical impedance spectroscopy (EIS). EIS uses a small alternating excitation signal that is applied across a sample. The resulting current is measured to allow calculation of the complex impedance. An alternating signal (AC) causes ions to move back and forth between counter and sample electrodes in response to the changing voltage magnitude and polarity. Thus, the AC polarization forces the electric double layer (EDL) of the corroding metal/electrolyte interface to change in response to the polarizing voltage frequency changes. However, because the EDL takes time to change its chemistry, it will have an associated time constant. Also, the EDL has electrical properties similar to those of a parallel resistor (R) capacitor (C) circuit where the time constant (T) is given by $T\ 1/f_{max} = CR2\pi$, where f_{max} is apex frequency of a plot of the imaginary and real components of the impedance. Therefore, by using an AC signal and measuring the complex impedance spectrum, the time constants of the corroding mechanisms that are occurring may be studied. The small excitation signal used, typically <20 mV, does not cause destructive effects to the coating or coating-metal interface. Extraction of the impedance characteristics of the sample allows the elucidation of an equivalent circuit model that describes the elements of the sample. Measurements as a function of time with equivalent circuit modeling then allow the corroding elements to be studied. So far these EIS techniques have been investigated primarily on organically coated metals (Ref 4).

Previous studies of sol-gel deposited coatings on stainless steel to prevent oxidation and chemical corrosion have included: Al_2O_3 (Ref 5), ZrO_2 (Ref 6-10), SiO_2 (Ref 11-13), TiO_2-SiO_2 (Ref 14, 15), SiO_2-Al_2O_3 (Ref 15), CeO_2 (Ref 16),

R.G. Biswas and **R.D. Sanders,** Department of Engineering, University of Warwick, Coventry, CV4 7AL, U.K.

and CeO_2-TiO_2 (Ref 16). The aqueous corrosion properties of some of these ceramic films have been studied by potentiodynamic polarization techniques (Ref 5, 6, 10) and by electrochemical impedance spectroscopy (Ref 10, 11).

Earlier studies of the benefits of a ceramic coating on stainless steel, based on electrochemical corrosion measurements, include: higher corrosion potential values (E_{corr}) for ZrO_2 coatings on 316L tested in 300 gram decimetre^{-3} H_2SO_4 (Ref 6), and for Al_2O_3 coatings on 316SS in 1M NaCl (Ref 5); and improved pitting resistance for CeO_2-coated Type 304 stainless steel (304SS) in de-aerated chloride environments (Ref 16), and for Al_2O_3 coatings on 316 (Ref 5). The CeO_2 coatings in these studies were obtained from solutions of cerium hydroxide colloidal solution (Ref 16) and by heat treating at 900 °C. Such high-temperature treatments, however, are known to be detrimental to austenitic stainless steel, due to the precipitation of carbides at the grain boundaries (Ref 17).

The work presented here shows a systematic study of the aqueous corrosion properties of heat-treated, inorganic sol-gel CeO_2 coatings on 304SS in 1M NaCl. Corrosion parameters are then derived for coated and uncoated stainless steel from potentiodynamic polarization measurements and electrochemical impedance spectroscopy measurements.

Table 1 Crystallite sizes determined by XRD for heat-treated CeO_2 coatings of 304SS

Heat treatment, °C	450	550	2 × 450
Crystallite size, nm	597	713	654

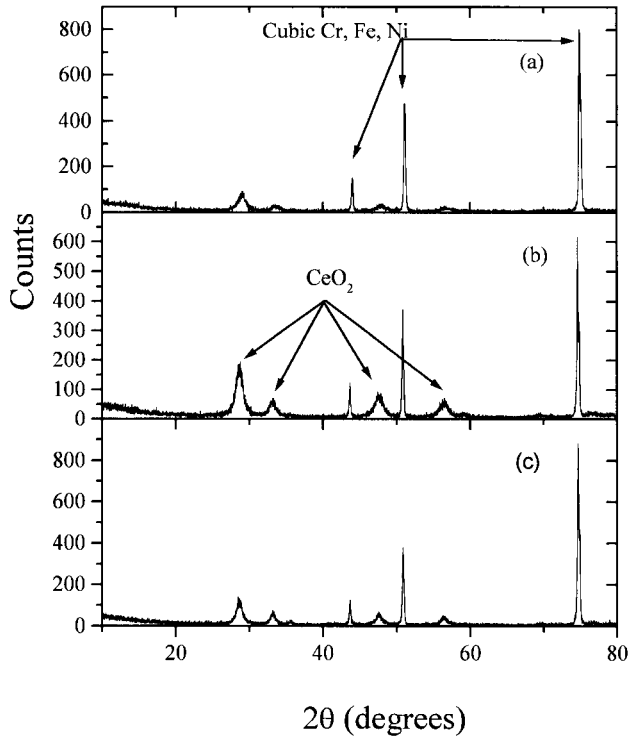

Fig. 1 XRD patterns of CeO_2-coated 304SS, (a) heat treated at 450 °C, (b) heat treated at 550 °C, (c) doubly coated and heat treated at 450 °C

2. Experimental Procedure

2.1 Sol Preparation

Ceria sols were prepared by using a method similar to that previously published (Ref 18), where a hydrous ceria oxide, $CeO_2 \cdot xH_2O$, was precipitated from the corresponding cerium (IV) salt using ammonia. This was washed and peptized with nitric acid to give a monodisperse sol with a 5 to 8 nm particle size determined from photon-correlation spectroscopy. For coating purposes, the sols were diluted to 80 gram decimetre^{-1} with a pH between 1.6 and 2.6. The sol was stable to precipitation and viscosity changes, and could be evaporated to form a transparent gel.

2.2 Metal Preparation

Type 304 stainless steel sheet with a bright annealed finish and a protective plastic coating on one side, supplied from Aalco (Ref 19), was diced using a guillotine into coupons of 30 by 45 by 1 mm, and 10 by 10 by 1 mm. The large coupons were used for corrosion experiments and optical microscopy while the smaller coupons were used for x-ray diffraction (XRD) measurements. Prior to application of the coating, the plastic coating was removed to reveal a scratch-free surface. The coupons were scrubbed with isopropyl alcohol, subjected to ten-minute ultrasonic treatment in an acetone bath, and then air dried.

2.3 Coating

Coupons were dip coated in the sol by hand and allowed to dry vertically in air. Only half of each coupon was dipped into the sol, so that the coated half could be compared against the uncoated half after temperature treatment. The excess sol that collected on the bottom edges of the coupon was towel-dried off. After air drying, the coupons were visually inspected for flaws and then stacked horizontally in an alumina boat and heat treated in air within a muffle furnace. Temperature treatments of 450 °C/1 h and 550 °C/1 h were used.

2.4 XRD Measurements

XRD patterns for the heat-treated coupons were recorded in the region $2\theta = 10 - 80°$, with a step scan of 0.1°/min on a Philips diffractometer (Phillips Analytical, The Netherlands; model PW1710) using CuKα radiation. The Philips APD1700 software (Phillips Analytical, The Netherlands) was used to calculate the average crystallite size from the broadening of a specific diffraction peak, using the well-known Scherrer equation, $D = k\lambda/h_{1/2}\cos\theta$, where D is the average crystallite size, k is the Scherrer constant, λ is the wavelength of radiation, $h_{1/2}$ is the peak width at half height, and θ corresponds to the peak position.

2.5 Corrosion Measurements

Potentiodynamic polarization measurements were performed using a computerized Solartron 1287 electrochemical interface controlled by CorrWare (Ref 20). Coupons were clamped against a silicone sealing ring with an area of 1.776

cm^2. A 1M NaCl electrolyte was used with a saturated calomel electrode as the reference electrode and platinum as the auxiliary electrode. Samples were left to stabilize at the open circuit potential (OCP) for 60 min before commencement of the potentiodynamic measurement. Polarization curves were then obtained by scanning the potential from –0.3 V of the OCP at a rate of 0.1667 mV/s until the anodic current of 1×10^{-3} A/cm^2 was reached. Data were obtained for cleaned, heat-treated coupons and for CeO_2-coated, heat-treated coupons. AC impedance spectroscopy measurements were performed using the Solartron 1287 and Solartron 1260 gain/phase impedance analyzer controlled by ZPlotW (Ref 20). Measurements were performed at the OCP between the frequencies of 0.03 Hz and 40 kHz, using an excitation voltage of 10 mV.

3. Results

After heat treatment, the coatings appeared to be transparent, adherent, and coherent. By coating microscope slides and then heat treating them at 450 °C, a coating thickness of 0.5 ± 0.1 μm was determined using a stylus technique. Figure 1 shows the XRD patterns for the coated 304SS coupons heat treated at 450 and 550 °C, and for a coupon doubly coated with CeO_2 and heat treated twice at 450 °C. The sharp peaks at 2θ = 43°, 50.8°, and 74.7° are due to the cubic phase of chromium, iron, and nickel (Ref 21), while the peaks at 2θ = 28.6°, 33.1°, 47.5°, and 56.4° are due to the cubic CeO_2 coating (Ref 22). The peak width indicates the formation of nanocrystallites. The peaks increase in intensity for the doubly coated specimen (Fig. 1c), while the crystallite size increases with sintering temperature and sintering time, as shown in Table 1.

Figure 2 shows the polarization curves obtained for the uncoated specimens: untreated, heat treated at 450 °C, and heat treated at 550 °C. The curves have been manipulated by filtering options in the CorrWare program to aid plotting, and were obtained after 60 min immersion in the electrolyte when the OCP had stabilized. For all the samples, the cathodic regions of the polarization curves show similar behavior, while the anodic regions show the greatest differences due to the heat treatments. The untreated coupon shows transpassive behavior. The 450 °C heat-treated sample shows similar behavior, but with lower current densities. The pitting potentials for the samples (E_{pitt}), defined as the potential where there is an abrupt rise in the current, are given in Table 2 and show that the E_{pitt} decreases with increasing heat treatment temperature. The 550 °C sample shows no apparent pitting potential and the current increases with potential throughout the entire anodic scan indicating that pitting can occur a few mV anodic of the OCP.

The corrosion parameters i_{corr} (corrosion current density in A/cm^2), E_{corr} (corrosion potential), and corrosion rate (CR in mm/year) have been obtained from polarization data by calculating the Tafel slopes using CorrWare (Ref 20). E_{corr} is the potential at which the anodic and cathodic Tafel slopes intersect and i_{corr} is the current at which the Tafel slopes intersect. The CR is then calculated from i_{corr}, using the expression $CR = i_{corr} EW 10/\rho 96500$, derived from Faraday's law, where EW is the equivalent weight of the corroding species and ρ is the density. The calculated data are given in Table 2.

Comparing the uncoated specimens, the CR is highest for the 550 °C heat-treated sample. The 450 °C sample shows the lowest CR and i_{corr} values, due to the formation of a thicker passive oxide layer.

The corrosion parameters calculated from the polarization curves for the CeO_2-coated coupons that were heat treated at 450 and 550 °C (Fig. 3) are given in Table 2. The polarization curves for the 450 °C coated and uncoated coupons show the largest difference in characteristics. The coated coupons show

Table 2 Electrochemical corrosion parameters for heat-treated 304SS in 1M NaCl derived from polarization curves given in Fig. 2 and 3

Sample	Epitt, mV	E_{corr}, mV	i_{corr}, A/cm^2	CR, mm/yr
As-received (cleaned)	671	–201	2.6×10^{-9}	2.7×10^{-5}
450 °C uncoated	476	–166	8.8×10^{-10}	9.3×10^{-6}
550 °C uncoated	…	–503	3.4×10^{-7}	2.8×10^{-3}
CeO_2 (450 °C)	700	–180	1.2×10^{-8}	1.2×10^{-4}
CeO_2 (550 °C)	…	–429	7.1×10^{-8}	7.4×10^{-4}

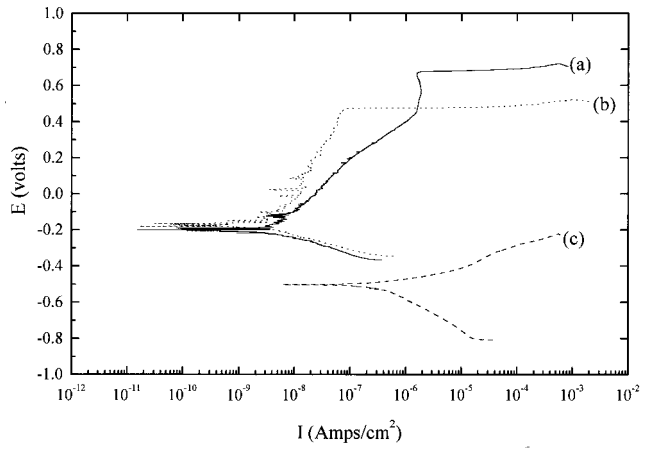

Fig. 2 Polarization curves for uncoated 304SS in 1M NaCl, (a) as-received (cleaned), (b) heat treated at 450 °C, (c) heat treated at 550 °C

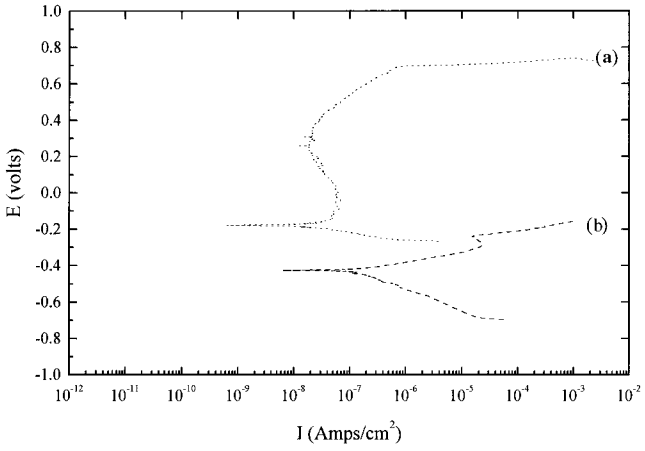

Fig. 3 Polarization curves for CeO_2-coated 304SS in 1M NaCl, (a) heat treated at 450 °C, (b) heat treated at 550 °C

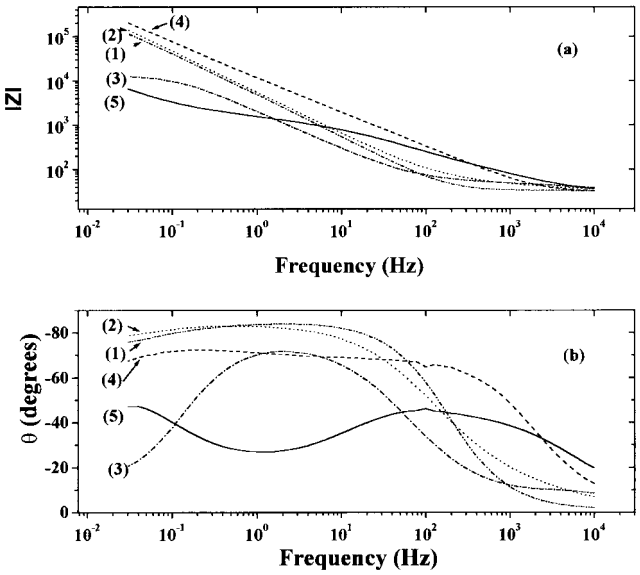

Fig. 4 Bode plot for uncoated and CeO_2-coated coupons. (a) Logarithm of the magnitude of the impedance modulus |Z| and (b) phase angle versus frequency. Curves: (1) 304SS untreated, (2) heat treated at 450 °C, (3) heat treated at 550 °C, (4) CeO_2-coated and heat treated at 450 °C, (5) CeO_2-coated and heat treated at 550 °C

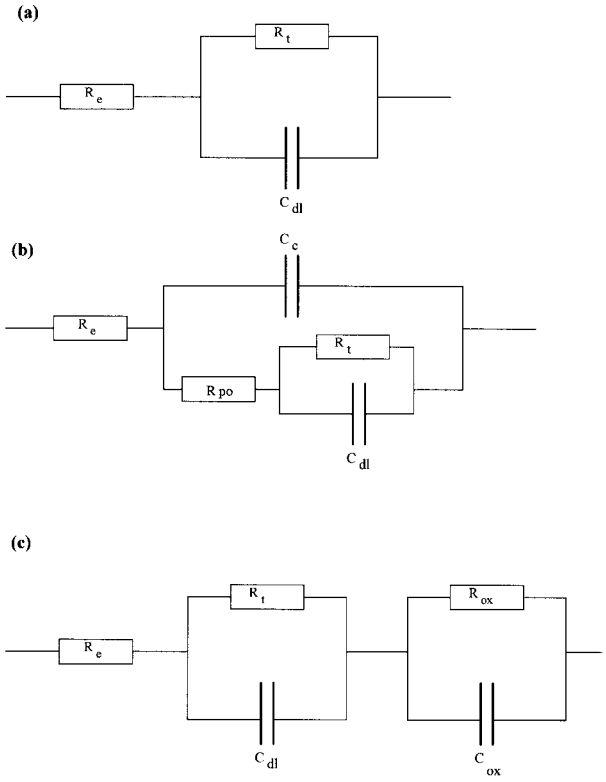

Fig. 5 Equivalent circuits used in analysis on impedance spectroscopy data. (a) Modified Randles circuit, (b) two time constants model, (c) model used for oxidized metal

a passive region for voltages between –50 and 330 mV. The E_{pitt} value for the 450 °C sample is the highest of all samples at 700 mV and is similar to the untreated metal. For voltages above 330 mV, the polarization behavior is "transpassive" until E_{pitt} is reached. The current density is also lower in the passive region of the coated sample than of the uncoated specimen. Comparison of the polarization curves for the 550 °C heat-treated coated and uncoated coupons shows that they have similar characteristics, although the CR and i_{corr} values are lower for the coated coupon.

To obtain further information about the influence of the CeO_2 coating on the corrosion behavior of heat-treated 304SS, EIS measurements were performed before commencement of the polarization measurements. The open circuit potential before and after the EIS measurements were very similar, indicating that there were no destructive effects due to the EIS measurement. The electrochemical impedance spectrum for the coated and uncoated specimens, heat treated at 450 and 500 °C, are plotted in the Bode format (logarithm of the magnitude of the impedance modules Z and the phase angle θ as a function of frequency) in Fig. 4. The data show that there is a wide variation in impedance characteristics according to the treatment of the 304SS. Generally, for simple corrosion systems that are entirely under charge transfer control, and for uniform corrosion on homogeneous surfaces, the equivalent circuit for modeling the impedance characteristics is given by a simple Randles circuit (Ref 23), as shown in Fig. 5(a). Using the Boukamp circuit description (Ref 24), the equivalent circuit can be written as $R_e(R_tC_{dl})$, where R_e is the resistance of the electrolyte solution and corrosion product film, C_{dl} is the electrochemical double layer due to absorbed ions and water molecules, and R_t is the polarization resistance. For real systems, there is usually a distribution of relaxation times which gives rise to distorted semicircles. This is represented in the Boukamp circuit description by substituting a constant phase element Q_{dl} for C_{dl}. For a simple corrosion system, then, R_t is equivalent to R_p, the linear polarization resistance which can be used in the Stern-Geary relationship to calculate the corrosion current density (i_{corr}). Observation of the Bode plots shows that for the uncoated, as-received (untreated) coupon, there is one time constant present (i.e., one parallel CR combination), and that the Randles circuit in Fig. 5(a) should be a suitable model. Fitting of the data using Boukamp's EQUIVCRT (Ref 24) yields the results in Table 3. The Bode plot for the 550 °C coated sample (Fig. 4a, b) shows that there are two time constants present.

The data are then best fitted to the model in Fig. 5(b), where the extra elements C_c and R_{po} represent the capacitance due to the coating and the pore resistance across the coating, respectively. Using the Boukamp circuit description, this is described as $R_e\{C_c[R_{po}(C_{dl}R_t)]\}$. Data fitting gives the results in Table 3 with $\chi^2 < 6 \times 10^{-3}$. Data for the 450 °C coated sample show characteristics similar to the untreated sample, and can thus be fitted with the Randles type equivalent circuit, the result of which is given in Table 2. Data for the uncoated 450 and 550 °C heat-treated coupons do not fit the Randles model. A best fit, however, is obtained using the model $R_e(R_tC_{dl})(R_{ox}C_{ox})$, as shown in Fig. 5(c), to give $\chi^2 < 5 \times 10^{-4}$. The equivalent circuit thus indicates that there is a layer that is in parallel and in series with the double layer capacitance, and is probably due to an oxide. This has been described by R_{ox} and C_{ox}. As expected, the

Table 3 Modeled fits to complex impedance spectrum for untreated 304SS, 450 °C and 550°C heat-treated uncoated 304SS, and 450 °C and 550 °C CeO_2-coated 304SS coupons

Untreated, $R_e(R_tQ_{dl})$		450 °C uncoated, $R_{et}(R_tQ_{dl}(R_{ox}Q_{ox})$		550 °C uncoated, $R_e(R_tQ_{dl})(R_{ox}Q_{ox})$		450 °C CeO_2-coated, $R_e(R_tC_{dl})$		550 °C CeO_2-coated, $R_e\{Q_c[R_{po}(Q_{dl}R_t)]\}$	
Element	**Value**	**Element**	**Value**	**Element**	**Value**	**Element**	**Value**	**Element**	**Value**
R_e	33Ω	R_e	32Ω	R_e	25.2Ω	R_e	28.6Ω	R_e	25Ω
R_t	$6.3 \times 10^5\Omega$	R_t	56Ω	R_t	47.1Ω	R_t	$8.2 \times 10^6\Omega$	Q_c	7.7×10^{-5}
Q_{dl}	3.7e–5	Q_{dl}	7.9×10^{-4}	Q_{dl}	1.5×10^{-3}	Q_{dl}	1.88×10^{-5}	n_c	0.61
n_{dl}	0.94	n_{dl}	0.48	n_{dl}	0.31	n_{dl}	0.8	R_{po}	$1.9 \times 10^3\Omega$
		R_{ox}	$1.4 \times 10^6\Omega$	R_{ox}	$1.5 \times 10^4\Omega$			Q_{dl}	4.6×10^{-4}
		Q_{ox}	3.2×10^{-5}	Q_{ox}	9.6×10^{-5}			n_{dl}	0.77
		n_{ox}	0.93	n_{ox}	0.87			R_t	$3.1 \times 10^{-4}\Omega$

fitted values of R_e are approximately the same in all the samples, as this is just the uncompensated solution resistance. The value of R_t calculated for the uncoated coupon is approximately of the same order of magnitude as the calculated polarization resistance $R_p = 8 \times 10^6\Omega$ from the DC polarization measurements.

Optical microscopy examination of the samples after electrochemical measurements was carried out on all samples using a Polylite Reichart microscope (C. Reichert Optische Werke, Austria). The untreated, as-received sample showed that four large pits had formed at apparently random points across the sample-electrolyte interface. The 450 °C uncoated sample showed three large pits of similar behavior, but with the oxide layer formed during the heat treatment still covering the surface. The 450 °C coated sample showed a higher density of pits, also at apparently random points across the sample-electrolyte interface. The CeO_2 coating was still in evidence across the sample. The 550 °C uncoated sample showed a complete absence of any oxide layer but with crevice corrosion occurring at the sealing ring interface with the sample. The 550 °C coated sample also showed some crevice corrosion occurring at the sealing ring interface. The CeO_2 coating, although still evident, showed some discoloration due to the production of corrosion products.

4. Conclusions

Films of CeO_2 deposited from an inorganic sol-gel precursor were applied onto 304 bright annealed stainless steel by dip coating. The coatings were sintered at temperatures of 450 and 550 °C to produce stable, transparent, and uniform films of crystalline CeO_2 with a thickness of 0.5 ± 0.1 μm. X-ray diffraction measurements confirmed that the films were crystalline with crystallite sizes between 600 and 715 nm. The anodic region of the polarization plot for the 450 °C coated coupon showed a passive region and transpassive behavior for potentials higher than 330 mV. The pitting potential was of the same order of magnitude as an untreated coupon. The uncoated 450 °C showed only transpassive behavior. The 550 °C heat-treated coupons (coated and uncoated) showed no passive type behavior. The calculated corrosion parameters indicated that the CeO_2 coating increased the CR and i_{corr} values for the 450 °C heat-treated specimen compared to the uncoated coupon. Heat treatment at 550 °C improved the CR of the coated coupon. EIS measurement indicated that the impedance spectrum for the untreated coupon may be modeled using a Randles type circuit. Modifying this circuit to include an element due to the capacitance of the coating allows the 550 °C coated sample to be modeled. The impedance spectrum for the heat-treated, uncoated coupons needs the addition of another capacitance and resistance element ($C_{ox}R_{ox}$) in series with the C_{dl} and R_t element for the equivalent circuit to be fitted sufficiently well. Optical examination of the sample-electrolyte interface after the electrochemical measurements indicated that the thermal oxide produced on the 550 °C uncoated specimen was removed while the 450 °C uncoated specimen showed the formation of etch pits, with the oxide layer otherwise intact. The CeO_2 coating remained on all the samples, but with etch pits occurring in the 450 °C heat-treated sample and crevice corrosion evident in the 550 °C heat-treated sample, with corrosion products evident at the sample-electrolyte interface.

Acknowledgments

Some of this work formed part of Mr. R.D. Sanders' third-year undergraduate project in the Department of Engineering, University of Warwick 1996/1997. Dr. R.G. Biswas wishes to thank Dr. A.K. Bhattacharaya for a research fellowship in the Centre for Catalytic Systems and Materials Engineering, Warwick Manufacturing Group, Department of Engineering. The authors also wish to thank Dr. G. Cooke in the Advanced SIMS Projects research group, Department of Physics, for coating thickness measurements using a Sloan DEKTAK 3030 (Sloan Technology Corporation, Santa Barbara, CA) and Professor Pedro-de Lima Neto, Institute of Physics and Chemistry of Sao Carlos, University of Sao Paulo, Brazil, for useful discussions on electrochemical corrosion measurements.

References

1. Gorham Advanced Materials Institute, Thermal Spray Coatings, Gorham, 1990
2. K.H. Stern, Ed., *Metallurgical and Ceramic Protective Coatings*, 1st ed., Chapman & Hall, 1996
3. R.L. Nelson, J.D.F. Ramsay, J.L. Woodhead, J.A. Cairns, and J.A.A. Crossley, *Thin Solid Films*, Vol 81, 1981, p 329-337
4. F. Mansfeld, *J. Appl. Electrochem.*, Vol 25, 1995, p 187
5. R.G. Biswas, J.L. Woodhead, and A.K. Bhattcharaya, *J. Mater. Sci. Lett.*, Vol 16, 1997, p 1628-1633
6. M. Atik, J. Zarzycki, and C. R'Kha, *J. Mater. Sci. Lett.*, Vol 13, 1994, p 266-269

7. K. Izumi, M. Murakami, T. Deguchi, A. Morita, N. Tohge, and T. Minami, *J. Am. Ceram. Soc.*, Vol 72, 1989, p 1465-1468
8. P. de L. Neto, M. Atik, L.A. Avaca, and M.A. Aegerter, *J. Sol-Gel Sci. Tech.*, Vol 1, 1994, p 177-184
9. M. Atik and M.A. Aegerter, *J. Non-Crystalline Solids*, Vol 147 and 148, 1992, p 813-819
10. P. de L. Neto, L.A. Avaca, M. Atik, M.A. Aegerter, and R.C. Rocha-Filho, *J. Braz. Chem. Soc.*, Vol 6, 1995, p 33-37
11. J. de Damorenea, N. Pellegri, O. de Sanctis, and A. Duran, *J. Sol-Gel Sci. Tech.*, Vol 4, 1995, p 239-244
12. O. de Sanctis, L. Gómez, N. Pellegri, C. Parodi, A. Marajofsky, and A. Duran, *J. Non-Crystalline Solids*, Vol 121, 1990, p 338-343
13. M. Atik, P. de L. Neto, L.A. Avaca, M.A. Aegerter, and J. Zarzycki, *J. Mater. Sci. Lett.*, Vol 13, 1994, p 1081-1085
14. M. Atik, P. de L. Neto, M.A. Aegerter, and L.A. Avaca, *J. Appl. Electrochem.*, Vol 25, 1995, p 142-148
15. P. De L. Neto, M. Atik, L.A. Avaca, and M.A. Aegerter, *J. Sol-Gel Sci. Tech.*, Vol 2, 1994, p 529-534
16. P.P Trzaskoma-Paulette and A. Nazeri, *Proc. Symp. Electrochemical Technology Applied to Environmental Problems*, E.W. Brooman, J.M. Fenton, and C. Hamel, Ed., Vol 95, 1995, p 207
17. D.A. Jones, *Principles and Prevention of Corrosion*, Prentice & Hall, Inc., 1996
18. A.K. Bhattcharaya, A. Hartridge, K.K. Mallick, and J.L. Woodhead, *J. Mater. Sci.*, Vol 31, 1996, p 5005-5007
19. Aalco, Halesowen, West Midlands, U.K. (supplier Type 304SS)
20. Scribner Associates, Inc., Charlottesville, Virginia (supplier of CorrWare and ZPlot corrosion software)
21. JCPDS, diffraction file 33-397
22. JCPDS, diffraction file 34-394
23. J.E.B. Randles, *Discuss Faraday Soc.*, Vol 1, 1947, p 11-19
24. B.A. Boukamp, *Equivalent Circuit*, Department Chemical Technology, University of Twente, The Netherlands, 1988/89